

An introduction to Langmuir probe diagnostics of plasmas

Luis Conde
Departamento de Física Aplicada
E.T.S. Ingenieros Aeronáuticos
Universidad Politécnica de Madrid
28040 Madrid, Spain.

May 28, 2011

Abstract

In this short review is introduced the elementary theory of collecting Langmuir probes in spherical and cylindrical geometries. The classical results for either repelled and attracted charges are deduced and the different approximations and limits of application are discussed with special insight in laboratory and practical applications. The principles and operation modes of emissive Langmuir probes are also discussed and also an updated bibliography is provided for further reading.

Contents

1	Introduction.	3
2	Qualitative description of collecting current voltage curves.	4
3	The simplified theory for collisionless unmagnetized plasmas.	8
3.1	Spherical probe	9
3.1.1	Repelled particles	10
3.1.2	Attracted particles	12
3.2	Cylindrical probe	13
3.2.1	Repelled particles	14
3.2.2	Attracted particles	15
3.3	Approximations	17
3.3.1	The thin sheath limit	17
3.3.2	The thick sheath limit	18
3.4	The energy distribution function of repelled particles	20

4	Interpretation of Langmuir probe data for repelling electrons	21
4.1	The analysis of experimental results	21
5	Emissive Langmuir probes	23
5.1	Floating emissive probe	24
5.2	The inflection point method	26

1 Introduction.

The Nobel laureate Irving Langmuir made outstanding contributions in different fields of Physics during the past century. He coined the term *plasma* in relation to the physics of partially ionized gases and also invented the *Langmuir probes* to measure the electron plasma density n_e , the space potential V_{sp} and the electron temperature $K_B T_e$ in cold low density plasmas.

These Langmuir probes are one of the different *electric probe diagnostics* that are employed today. In a broader sense, the electric probes measure the local plasma parameters by using stationary or slow time varying electric (and/or magnetic) fields to emit or to collect charged particles from the plasma. These measuring techniques constitute an active field of research and are particularly well suited for low density cold plasmas, as low pressure electric discharges, ionospheric and space plasmas.

The simplest collecting Langmuir probe is a metallic electrode (as those of Fig. 1) with a well defined geometry (planar, cylindrical or spherical). The probe is immersed into the plasma and polarized to the potential V_p by an external circuit. This bias to $V = V_p - V_{sp}$ the probe with respect to the local space plasma potential V_{sp} . Then, the drained current $I_p = I(V_p)$ for different probe potentials V_p is monitored and the plasma parameters are calculated from this *voltage - current* (IV) characteristic curves.

However, behind this apparently simple scheme are hidden the intricate theoretical and practical problems involved in the charge collection processes from a plasma.

The plasma parameters are deduced from the current I_p , which, in accordance to the bias voltage $V = V_p - V_{sp}$ is composed of ions, electrons or both. The attracted charges are collected by through the electric field between the bulk plasma and the metallic surface of the probe. This undetermined spatial potential profile extends in the plasma along distances in the order of few Debye lengths λ_D and is denominated *plasma sheath*. In addition, this local electric field also may be altered according to the magnitude of the current I_p collected.

Therefore, the charge collection process depends on different characteristic lengths, as the probe size r_p and the thickness (or spatial extension) of the plasma sheath attached to the collecting surface, which related with λ_D . In magnetized plasmas the electron r_e and ion r_i Larmor radius also introduce additional lengths,

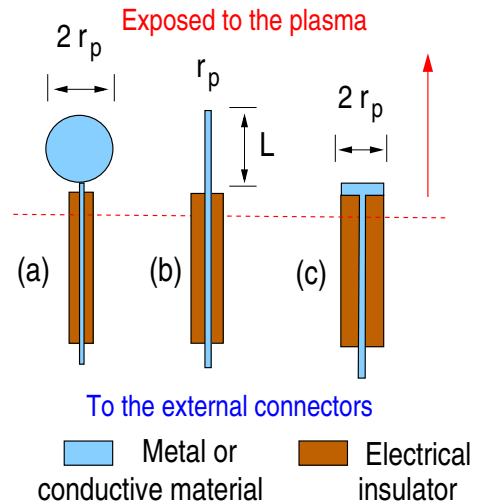


Figure 1: Collecting Langmuir probes with radius r_p and (a) spherical, (b) cylindrical and (c) planar geometries.

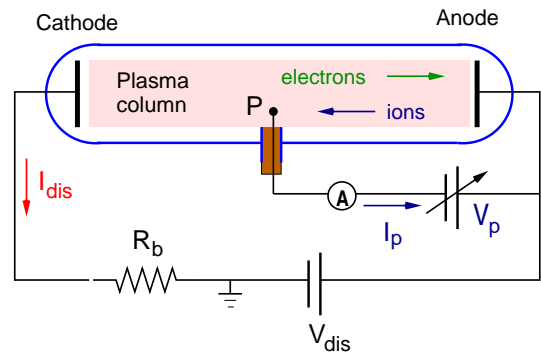


Figure 2: Scheme of the of the circuit for probe measurements in a glow discharge.

as well as the mean free paths λ for collisions between electrons and/or ions and neutral atoms in collisional and weakly ionized plasmas.

The disparity between these magnitudes, that may differ by orders of magnitude for the different plasmas in nature and/or in measuring systems, leads the theory of Langmuir probes unfortunately incomplete. In fact, no general model is available relating the current voltage curves $I(V_p)$ with the actual plasma properties under all possible physical conditions.

For unmagnetized Maxwellian plasmas the simplified theory developed by Langmuir and Harold M. Mott-Smith in 1926 allows under ideal conditions to determine the plasma potential V_{sp} , electron temperature $K_B T_e$ and density $n_e \simeq n_i$. The interpretation of the measurements outside the narrow limits of this simplified theory is difficult and many points still remains obscure.

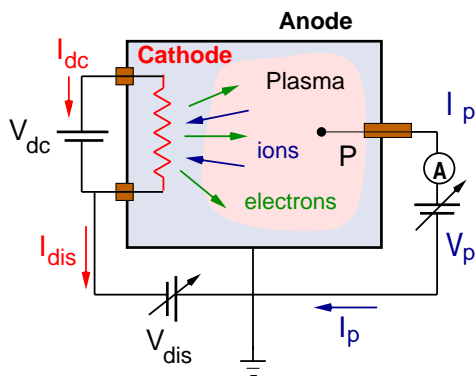


Figure 3: Scheme of the of the circuit for probe measurements in a plasma produced by thermionic emission of electrons.

The idealized situation where the simplified theory strictly applies is seldom found in the experiments of interest. However, even in these situations where different drifting populations of charged particles are present or under intense magnetic fields the electric probes may provide valuable information.

The reader will find these notes as incomplete because they only cover a limited number of topics on Langmuir probe theory. The fundamentals are introduced with a detailed deduction of the relevant expressions, however, they do not intend to replace the excellent monographs and reviews existing in the literature [1, 2, 3, 5]. Our aim is to facilitate to our students an starting point and more involved models are left for further readings.

2 Qualitative description of collecting current voltage curves.

The Figs. 2 and 3 represents the two simplest measurement circuits using collecting Langmuir probes in experiments with cold weakly ionized plasmas. The first case is a *glow discharge* plasma into a glass tube (or other gas evacuated vessel) with typical pressures between $10^{-2} - 10^2$ mBar. The electric discharge is produced by applying a high DC voltage V_{dis} (between 300-600 Volts or more) and the corresponding discharge current I_{dis} is in the range of 0.1 – 100 mA. The physical properties of the *glow discharge* and other electric discharges are discussed in detail in Ref. [3].

In the scheme of Fig. 3 the wires heated up to red glow by a DC current I_h inside the vacuum chamber to produce the thermoionic emission of electrons. These electrons are later accelerated by a discharge voltage $V_{dis} \sim 20 - 80$ Volts, over the first ionization potential of the neutral gas, and cause the electron impact ionization of the neutral atoms remaining in the vacuum chamber. In this case, the discharge current I_{dis} may reach several amps and additional permanent magnets (not shown in the picture) are frequently disposed around the plasma chamber. This confines the electrons and enhance the local ionization.

In both cases, the probe P is immersed at a given point within the plasma biased to the electric potential V_p with respect to a reference electrode. The anode of the discharge is used in Figs. 2 and 3. However the cathode or the grounded metallic wall of the plasma chamber could also serve for reference electrode in other situations.

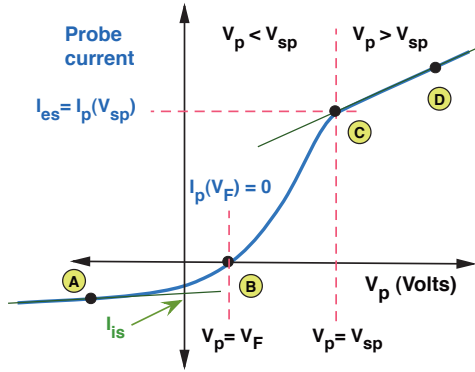


Figure 4: An idealized IV curve of obtained with a collecting Langmuir probe in a cold plasma. the electron temperature $K_B T_e \gg K_B T_i \simeq K_B T_a$ is higher than those of ions and neutrals.

The potential V_{sp} in Fig. 4 corresponds to the electric potential at the point of the plasma where the probe is inserted. The collecting probe do not emit particles, and in accordance to the potential V_p , the drained current $I_p = I_i + I_e$ from the plasma is composed of an ion I_i and electron I_e currents.

For very negative bias voltages $V_p \ll V_{sp}$ (at the left of point A in Fig.4) the electrons are repelled, while ions are attracted by the probe. The drained ion current from the plasma is limited by the electric shielding of the probe and I_p decreases slowly for very negative $V_p \ll V_{sp}$. The current $I_p \simeq I_{is}$ is denominated *ion saturation current*.

In the opposite limit (voltages at the right of point C in Fig. 4) where $V_p \gg V_{sp}$ the ions are repelled and the electrons are the attracted charges. In this case the electrons are responsible for the electric shielding of the probe and $I_p \simeq I_{es}$ is called the *electron saturation current*. The bias potential V_F where $I_p = 0$ is the *floating potential* (point B) where the contributions of the ion and electron currents are equals.

The situation where $V_p \ll V_{sp}$ is shown in the scheme of Fig. 5 only an small number of electrons have energy enough to jump the potential barrier of V_p . The ions are attracted to the probe and a *layer* of negative space charge (*negative sheath*) develops for $r < r_s$ attached to the metallic surface.

The potential drop from V_{sp} to V_p and the perturbation caused by the probe electric field is concentrated within the space charge layer around the probe, decreases asymptotically in

In the following, we will refer to a general probe as those of Fig. 1 with a characteristic length r_p . We will specify if the probe is either, spherical, cylindrical or planar only when geometry dependent properties are relevant.

The *current-voltage curves* (IV) are obtained by measuring the drained current I_p by the probe for each bias potential V_p and Fig. 4 represents an idealized voltage current (IV) curve.

In order to give a qualitative interpretation we will consider an idealized non equilibrium collisionless, Maxwellian and unmagnetized plasma. Thus, the collisional mean free paths of all particles are larger than all characteristic lengths ($\lambda \gg r_p, \lambda_D$) and also

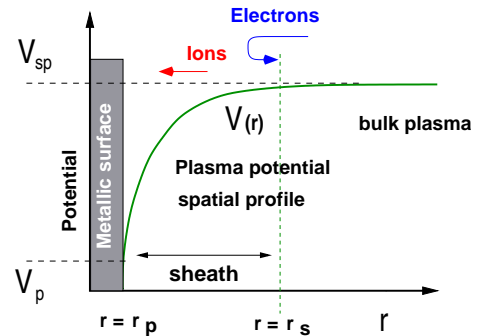


Figure 5: Radial potential profile attached to an ion collecting metallic surface.

the transition to the unperturbed plasma. The Fig. 6 represents the opposite situation with $V_p \gg V_{sp}$ where the attracted particles are electrons and again the *negative sheath* for $r < r_s$ connects the space potential of the unperturbed bulk plasma with V_p .

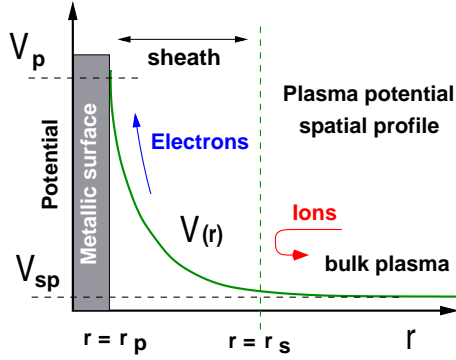


Figure 6: Radial potential profile attached to an electron collecting metallic surface.

The electrons (or ions) are brought from the bulk plasma to this boundary mostly by *thermal motion*. This factor determines the flux of charged particles crossing the radius $r_s > r_p$ towards the probe.

Therefore, the *attracted charges* are collected *over the surface defined by r_s* which could not be precisely calculated without solving the Poisson equation to determine $V(r)$. This will be a key point for attracted particles which enter in the plasma sheath over a surface with an undetermined radius $r_s > r_p$.

This effect is quite similar to the plasma polarization around a point charge where the spatial fluctuations of the plasma potential,

$$\delta V_{sp} \sim (1/r) \times \exp(-r/\lambda_D),$$

that exponentially decreases with the radial distance. Thus, the thickness of the sheath in Figs. 5 and 6 and therefore, the perturbation over the distance r_p introduced in the plasma by the probe is restricted to a few Debye lengths ¹.

The vertical dotted lines in Figs. 5 and 6 represents the external surface of the sheath r_s around the probe. This boundary is not accurately determined and is the limit beyond the plasma could be considered again

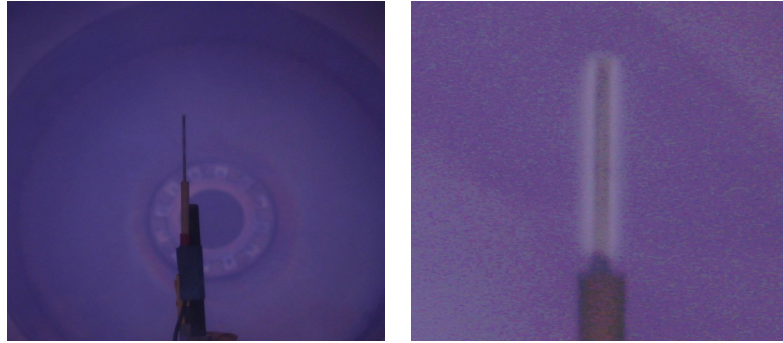


Figure 7: A cylindrical probe operating in a glow discharge plasma (left) and a closer view for large positive bias (right). In weakly ionized plasmas, this glow is produced for $V_p \gg V_{sp}$ by the inelastic collisions between neutral atoms and attracted electrons in the sheath.

The *plasma sheath* formed by attracted electrons can be visualized in a weakly ionized plasma by the bright glow surrounding the cylindrical probe in Fig. 7. Because of the large neutral gas atom density, the inelastic collisions of neutrals with the accelerated electrons in the sheath produce the emission of light. The large electron currents heat the probe and this fact is also used for probe surface cleaning.

¹The structure of the ion sheath is discussed in detail in Sec. 8.2 pp. 290-295 of Ref. [4].

On the contrary, the *repelled charges* with thermal energy enough to overcome the potential barrier and to reach the probe *are collected over its surface*. The drained current I_p of attracted particles (for either $V_p \gg V_{sp}$ and $V_p \ll V_{sp}$) becomes therefore *weakly dependent of V_p* as shown in Fig. 4. This saturation process by attracted particles is in the origin of the currents I_{is} and I_{es} which are respectively the *ion* and *electron saturation currents*.

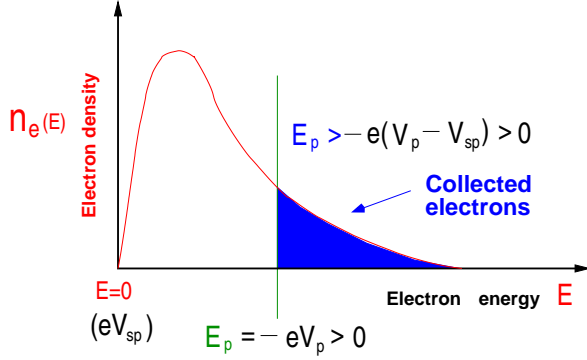


Figure 8: Electron collection process in the retarding field region (curve BC) of Fig. 4.

ing of I_p in Fig. 4 between B and C which is *strongly dependent of V_p* , contrary to the current saturation processes (over point C and below B). This part of the IV curve is frequently denominated *electron retarding field* because the probe bias V_p repels a fraction of electrons from reaching the probe.

Finally, when $V_p = V_{sp}$ no sheath develops around the probe and the charges reach its surface because of their thermal motion. Thus, the probe collects the thermal flux of both electrons $\Gamma_{e,Th}$ and ions $\Gamma_{i,Th}$. In consequence, the probe biased at the space plasma potential *drains an electric current* from the plasma even *in the absence of potential difference* between the conductor and the surrounding plasma.

The thermal flux of electrons ($\alpha = e$) and ($\alpha = i$) ions is given by,

$$\Gamma_{\alpha,Th} = \frac{1}{4} n_{\alpha} \left(\frac{8K_B T_e}{\pi m_{\alpha}} \right)^{1/2}$$

and their density currents are, $I_{\alpha,Th} = q_{\alpha} \Gamma_{\alpha,Th}$. Because, $m_i \gg m_e$ and $K_B T_e \gg K_B T_i$ on practical grounds,

$$I_p = I_{e,Th} + I_{i,Th} = I_{e,Th} \left(1 + \frac{I_{i,Th}}{I_{e,Th}} \right) \simeq I_{e,Th}$$

and therefore, the current $I_p(V_p)$ in Fig. 4 is equal to the electron thermal and saturation currents $I_p(V_p) \simeq I_{et} = I_{es} \gg I_{is}$.

The next step is to calculate the plasma parameters from the IV curve fitting obtained in the experiments. This requires of physical models relating the drained current I_p with the energy distribution functions of charged particles. Unfortunately, because of the wide range of plasma densities, temperatures and characteristic lengths the results are quite unrealistic if the wrong model is employed.

The electrons are repelled for probe bias $V_p - V_{sp} < 0$ below the local plasma potential. The Fig. 8 represents the fraction of collected electron with energy enough to reach the probe because of the finite electron temperature $K_B T_e$ of the Maxwellian energy distribution.

The number of electrons with energy,

$$E = -e(V_p - V_{sp}) \geq 0$$

that reach the probe increases as the bias $V_p - V_{sp}$ with respect to the bulk plasma decreases. This fact explains the abrupt growing of I_p in Fig. 4 between B and C which is *strongly dependent of V_p* , contrary to the current saturation processes (over point C and below B).

This part of the IV curve is frequently denominated *electron retarding field* because the probe bias V_p repels a fraction of electrons from reaching the probe.

Finally, when $V_p = V_{sp}$ no sheath develops around the probe and the charges reach its surface because of their thermal motion.

Thus, the probe collects the thermal flux of both electrons $\Gamma_{e,Th}$ and ions $\Gamma_{i,Th}$. In consequence, the probe biased at the space plasma potential *drains an electric current* from the plasma even *in the absence of potential difference* between the conductor and the surrounding plasma.

The thermal flux of electrons ($\alpha = e$) and ($\alpha = i$) ions is given by,

$$\Gamma_{\alpha,Th} = \frac{1}{4} n_{\alpha} \left(\frac{8K_B T_e}{\pi m_{\alpha}} \right)^{1/2}$$

and their density currents are, $I_{\alpha,Th} = q_{\alpha} \Gamma_{\alpha,Th}$. Because, $m_i \gg m_e$ and $K_B T_e \gg K_B T_i$ on practical grounds,

$$I_p = I_{e,Th} + I_{i,Th} = I_{e,Th} \left(1 + \frac{I_{i,Th}}{I_{e,Th}} \right) \simeq I_{e,Th}$$

and therefore, the current $I_p(V_p)$ in Fig. 4 is equal to the electron thermal and saturation currents $I_p(V_p) \simeq I_{et} = I_{es} \gg I_{is}$.

The next step is to calculate the plasma parameters from the IV curve fitting obtained in the experiments. This requires of physical models relating the drained current I_p with the energy distribution functions of charged particles. Unfortunately, because of the wide range of plasma densities, temperatures and characteristic lengths the results are quite unrealistic if the wrong model is employed.

3 The simplified theory for collisionless unmagnetized plasmas.

The simplest model relating the plasma properties with current voltage curves was formulated by Langmuir and Mott-Smith and is valid for unmagnetized collisionless Maxwellian plasmas. The following formulation of the theory essentially comes from Ref. [5] and these calculations rely on some assumptions that apply to most of nonequilibrium laboratory plasmas.

1. The bulk plasma volume is considered as infinite, stationary, homogeneous and quasineutral $n_e \simeq n_i$.
2. Electron and ions have Maxwellian distributions of velocities and the kinetic temperature of the species are $K_B T_e \gg K_B T_i \simeq K_B T_a$, where $\alpha = e, i, a$ represents respectively electrons, ions and neutral atoms.
3. The collisional mean free paths of electrons λ_e and ions λ_i are larger than r_p and λ_D .
4. The charged particles that reach the surface of the probe do not chemically react with the probe material, are always collected and contribute to the probe current $I(V_p)$.
5. The perturbation introduced by the probe in the plasma is confined to a space charge sheath with a well defined boundary. Outside this sheath the space potential is assumed uniform in the bulk plasma.
6. The sheath thickness $d \ll r_p$ is small compared with the characteristic probe dimension and therefore edge effects may be neglected.
7. The potential around the probe preserves the symmetry (spherical, cylindrical or planar) and $V(r)$ is a monotonically decreasing (or increasing) function between the sheath edge and the probe surface.

First of all, we will consider the motion of a charge q_α ($\alpha = e, i$) of mass m_α , located at the radial distance r with initial speed \mathbf{v} . This particle moves close to a cylindrical or spherical probe and we will use in the following $e = |e| > 0$, then $q_e = -e$ for electrons and $q_i = +e$ for ions.

The bulk plasma is considered as stationary and uniform in space (see previous points 1, 3 and 5) and the plasma potential takes an uniform value V_{sp} . For the a radial distance r the electric potential with respect to this undisturbed plasma is $\phi(r) = V(r) - V_{sp}$ and the probe potential is $\phi_p = V(r_p) - V_{sp}$.

It is of worth to recall that the plasma potential profile around the probe $\phi(r) = V(r) - V_{sp}$ remains undetermined. The only requisite (see previous points 5, 6 and 7) for the sheath potential $\phi(r)$ is to be a monotonic function decreasing or increasing fast enough close to the probe surface as in Figs. 5 and 6.

Two different situations arise, the charge q_α could be *repelled* by the *retarding electric field* around the probe when $q_\alpha \phi(r) > 0$. For electrons corresponds to the *BC* part of the IV curve of Fig. 4). On the contrary, the particle may be also *attracted* by the *accelerating field* when $q_\alpha \phi(r) < 0$ (in Fig. 4 the parts *AB* for ions and *CD* for electrons).

3.1 Spherical probe

In the case of the spherical probe, the motion of a single charge is restricted to a plane defined by its velocity \mathbf{v} and the plane of symmetry of the sphere. As in Fig. 9, the speed $\mathbf{v} = \mathbf{v}_\perp + \mathbf{v}_\parallel$ has two components \mathbf{v}_\parallel parallel and perpendicular \mathbf{v}_\perp to the radial direction \mathbf{e}_r , normal to the probe surface. The charge that reaches the probe surface r_p with speed $\mathbf{v}' = \mathbf{v}'_\parallel + \mathbf{v}'_\perp$ comes from the radial distance $r \geq r_p$ with the initial velocity \mathbf{v} .

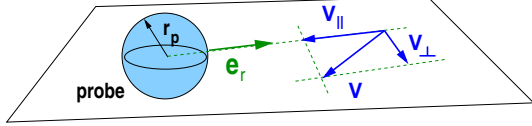


Figure 9: The scheme of the spherical probe and the components of the charge velocity.

In the absence of collisions the energy of this particle is conserved,

$$\frac{m_\alpha}{2}(v_\parallel^2 + v_\perp^2) + q_\alpha V_{sp} = \frac{m_\alpha}{2}(v_\parallel'^2 + v_\perp'^2) + q_\alpha V_p$$

and also for the component of the angular momentum perpendicular to the plane of Figs. 9 and 10,

$$r v_\perp = r_p v'_\perp \quad \text{and,} \quad v'_\perp = \frac{r}{r_p} v_\perp$$

Setting $\phi_p = V_p - V_{sp}$ we have,

$$v'^2 = v_\parallel^2 + v_\perp^2 \left(1 - \frac{r^2}{r_p^2}\right) - \frac{2q_\alpha}{m_\alpha} \phi_p \geq 0$$

In order to be collected $v' \geq 0$ and this relates the magnitude of the angular v_\perp and radial v_\parallel components of the velocity of collected charges,

$$v_\perp^2 \leq \frac{v_\parallel^2 - 2q_\alpha \phi_p / m_\alpha}{(r/r_p)^2 - 1}$$

As shown in Fig. 10 the components of the speed are, $v_\perp = v \sin \varphi$ and $v_\parallel = v \cos \varphi$,

$$v^2 \sin^2 \varphi \leq \frac{v_\parallel^2 - 2q_\alpha \phi_p / m_\alpha}{(r/r_p)^2 - 1}$$

From this expression we obtain the maximum allowed angle φ_m of the particle velocity \mathbf{v} with the radial direction \mathbf{e}_r of Fig. 10 for the distance r ,

$$\sin^2 \varphi_m \leq \frac{r_p^2}{r^2} \left(1 - \frac{2q_\alpha \phi_p}{m_\alpha v^2}\right) = \frac{r_p^2}{r^2} \left(1 - \frac{q_\alpha \phi_p}{E}\right) \quad (1)$$

This latter depends on the radial distance r to the probe and the ratio between the electrostatic energy ($q_\alpha \phi_p$) and the initial kinetic energy E of the incoming charge.

The key point of collecting Langmuir probe theory is to relate the energy spectrum of the attracted or repelled particles with current drained by the probe. Therefore, in order to relate

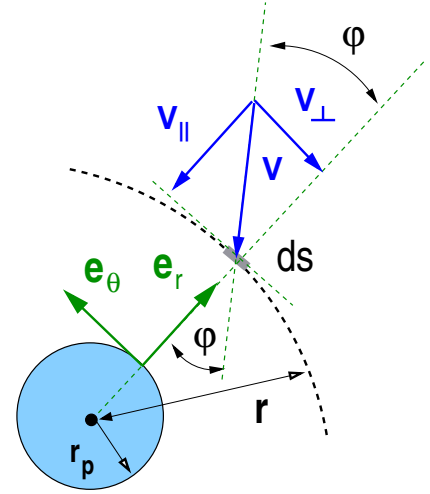


Figure 10: The velocity $\mathbf{v} = \mathbf{v}_\parallel + \mathbf{v}_\perp$ of the charge crossing the surface element $d\mathbf{S}$ placed at the radial distance r .

$I(r_p)$ with the plasma properties, instead of a monoenergetic charged particle, we consider a *velocity distribution function* $f_\alpha(\mathbf{v})$. Then, for each charged specie in the plasma,

$$dn_\alpha = n_{\alpha o} f_\alpha(\mathbf{v}) d\mathbf{v}$$

represents the number of particles by volume unit of the specie α with velocities between \mathbf{v} and $\mathbf{v} + d\mathbf{v}$. The above distribution function $f_\alpha(\mathbf{v})$ is normalized to,

$$\int_{-\infty}^{+\infty} f_\alpha(\mathbf{v}) d^3v = 1$$

and $n_{\alpha o}$ represents the density of particles of the specie α in the undisturbed bulk plasma.

3.1.1 Repelled particles

For *repelled* particles $q_\alpha \phi_p > 0$ and positive values of Eq. (1) require the kinetic energy of charges $E \geq q_\alpha \phi_p$, also $r \geq r_p$ for $\sin^2 \varphi \leq 1$. Therefore, the probe collects over its surface only the repelled particles with energy enough to overcome the potential barrier.

Because of the symmetry, the current density $d\mathbf{j}(r)$ over $d\mathbf{S}$ in Figs. 10 and 11 of charges attracted or repelled by the spherical is parallel fo \mathbf{e}_r and,

$$(d\mathbf{j})_{\parallel} = dj = q_\alpha v_{\parallel} dn_\alpha$$

The details of the integration over the surface $d\mathbf{S}$ are in Fig. 11, and using $d\mathbf{v} = v^2 \sin \varphi d\theta d\varphi dv$ we have,

$$dj = (q_\alpha n_{\alpha o}) (v \cos \varphi) v^2 \sin \varphi f_\alpha(\mathbf{v}) dv d\theta d\varphi \quad (2)$$

Now, we make an important assumption: *the velocity distribution function is isotropic*, only depends of the *energy* of particles, $f_\alpha(\mathbf{v}) = f_\alpha(|\mathbf{v}|)$, we obtain,

$$j(r) = (q_\alpha n_{\alpha o}) \int_{v_m}^{\infty} v^3 f_\alpha(v) dv \int_0^{2\pi} d\theta \int_0^{\varphi_m} \sin \varphi \cos \varphi d\varphi$$

For *repelled* charges ($q_\alpha \phi_p > 0$) a minimum initial energy (or speed) $mv_m^2/2 \geq q_\alpha \phi_p$ is necessary to overcome the potential barrier around the probe. Therefore,

$$j(r) = (q_\alpha n_{\alpha o}) \pi \int_{v_m}^{\infty} v^3 f_\alpha(v) \sin^2 \varphi_m dv$$

and $\sin \varphi_m$ is eliminated by using Eq. (1),

$$j(r) = (q_\alpha n_{\alpha o}) \pi \left(\frac{r_p^2}{r^2} \right) \int_{\sqrt{2q_\alpha \phi_p / m_\alpha}}^{\infty} v^3 f_\alpha(v) \left(1 - \frac{2q_\alpha \phi_p}{m_\alpha v^2} \right) dv \quad (3)$$

This last expression only depends on the particle velocity v and decreases with the radial distance. In the absence of ionizations and charge losses for $r \geq r_p$ for particles with $v \geq v_m$ the probe current is, $I(r) = I(r_p)$ and $I(r_p) = (4\pi r_p^2) j(r)$ and finally we have,

$$I(r_p) = (q_\alpha n_{\alpha o}) \pi A_{sph} \int_{\sqrt{2q_\alpha \phi_p / m_\alpha}}^{\infty} v^3 f_\alpha(v) \left(1 - \frac{2q_\alpha \phi_p}{m_\alpha v^2}\right) dv \quad (4)$$

where $A_{sph} = 4\pi r_p^2$ is the area of the spherical probe.

The Eqs. (3) and (4) are usually made dimensionless using the thermal speed,

$$c = \sqrt{\frac{2K_B T_\alpha}{m_\alpha}}$$

where $K_B T_\alpha$ is the kinetic temperature of the specie α . The scaled velocity is $\hat{u} = v/c$ and $\hat{u}_m = \sqrt{\hat{\phi}_p}$ with $\hat{\phi}_p = q\phi_p / K_B T_\alpha$. This dimensionless probe potential compares the electrostatic ($e\phi_p$) and thermal ($K_B T_\alpha$) energies of particles. Thus,

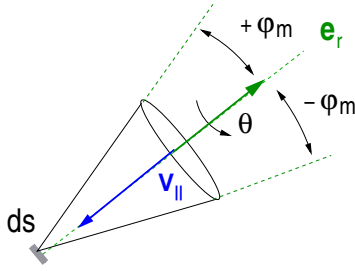


Figure 11: The angles considered over a surface element dS in Eq.(2).

$$j(r) = (q_\alpha n_{\alpha o}) \pi c^4 \left(\frac{r_p^2}{r^2}\right) \int_{\sqrt{\hat{\phi}_p}}^{\infty} \hat{u}^3 f_\alpha(\hat{u}) \left(1 - \frac{\hat{\phi}_p}{\hat{u}^2}\right) d\hat{u} \quad (5)$$

The above integrals could be evaluated for the particular case of the Maxwell Boltzmann velocity distribution function,

$$f(\hat{u}) = \frac{1}{\pi^{3/2} c^3} e^{-\hat{u}^2} \quad (6)$$

Using,

$$\int_{\hat{u}_m}^{\infty} \hat{u}^3 e^{-\hat{u}^2} \left(1 - \frac{\hat{u}_m^2}{\hat{u}^2}\right) d\hat{u} = \frac{e^{-\hat{u}_m^2}}{2}$$

we obtain a simple expression for the current of repelled particles,

$$j(r) = \frac{q_\alpha n_{\alpha o}}{4} V_{th} \exp\left(\frac{q_\alpha (V_{sp} - V_p)}{K_B T_\alpha}\right) \quad (7)$$

where $V_{th} = (8K_B T_\alpha / \pi m_\alpha)^{1/2}$ and also,

$$I(r_p) = \frac{q_\alpha n_{\alpha o} A_{sph}}{4} V_{th} \exp\left(\frac{q_\alpha (V_{sp} - V_p)}{K_B T_\alpha}\right) \quad (8)$$

This exponential growth of the current is in accordance with the expected response for electrons of the ideal probe along the segment BC in Fig. 4. When the probe is biased at the local plasma potential ($V_p = V_{sp}$ or $\phi_p = 0$) the current collected is the random flux of charges to its surface,

$$I(V_p) = \frac{q_\alpha n_{\alpha o} A_{sph}}{4} V_{th} \quad (9)$$

3.1.2 Attracted particles

For *attracted* charges setting $q_\alpha\phi_p = -|q_\alpha\phi_p| < 0$ in Eq. (1),

$$\sin^2 \varphi_m \leq \frac{r_p^2}{r^2} \left(1 + \frac{2|q_\alpha\phi_p|}{m_\alpha v^2} \right) = \frac{r_p^2}{r^2} \left(1 + \frac{|q_\alpha\phi_p|}{E} \right) \quad (10)$$

Thus, the behavior of the particle orbits depend on whether the initial particle velocities are smaller or larger than a certain velocity v_s defined by the radial distance,

$$r_s = r_p \sqrt{1 + \frac{|q_\alpha\phi_p|}{E}}$$

which is $r_s > r_p$ for $E > 0$. For a fixed (and at this point undetermined) value of r_s the speed v_s from Eq. (10) is,

$$v_s^2 = \frac{2|q_\alpha\phi_p|}{m_\alpha(r_s^2/r_p^2 - 1)}$$

that defines the energy $E_s = m_\alpha v_s^2/2$ leading $\sin \varphi_m = 1$ in Eq. (10).

The radial distance r_s , that could be identified with the *sheath threshold* of Figs. 5 and 6, and cannot be precisely determined at this point without solving the Poisson equation to determine the plasma potential profile $\phi(r)$ around the probe.

Therefore, for $r = r_s$ the particles with $E \leq E_s$ are collected because the Eq. (10) is always satisfied. The radial distance r_s plays the role of threshold radius for the particle orbits and the motion of the charges to the probe is said *sheath limited*. For $v > v_s$ and $r = r_s$ only those particles with $\sin^2 \varphi \leq 1$ are collected while others orbit or their trajectories bend around the probe. The motion of the charges is said to be *orbit limited*.

For *accelerated particles* the current density $d\mathbf{j}_\parallel(r)$ going into $d\mathbf{S}$ in Figs. 10 and 11 is composed of two terms, $dj(r_s) = dj_{sl}(r_s) + dj_{ol}(r_s)$ according to the velocity of the incoming charges with,

$$j_{sl}(r_s) = (q_\alpha n_{\alpha o}) \int_0^{v_s} v^3 f_\alpha(v) dv \int_0^{2\pi} d\theta \int_0^\pi \sin \varphi \cos \varphi d\varphi$$

also,

$$j_{ol}(r_s) = (q_\alpha n_{\alpha o}) \int_{v_s}^\infty v^3 f_\alpha(v) dv \int_0^{2\pi} d\theta \int_0^{\varphi_m} \sin \varphi \cos \varphi d\varphi$$

After the integration and using Eq. (10) for $\sin^2 \varphi_m$ we have,

$$j(r_s) = (q_\alpha n_{\alpha o}) \pi \left[\int_0^{v_s} v^3 f_\alpha(v) dv + \left(\frac{r_p^2}{r_s^2} \right) \int_{v_s}^\infty v^3 f_\alpha(v) \left(1 + \frac{2|q_\alpha\phi_p|}{m_\alpha v^2} \right) dv \right] \quad (11)$$

As before, the probe current is $I(r_p) = 4\pi r_s^2 j(r_s)$ and then,

$$I(r_p) = (q_\alpha n_{\alpha o}) \pi \left[(4\pi r_s^2) \int_0^{v_s} v^3 f_\alpha(v) dv + (4\pi r_p^2) \int_{v_s}^\infty v^3 f_\alpha(v) \left(1 + \frac{2|q_\alpha\phi_p|}{m_\alpha v^2} \right) dv \right] \quad (12)$$

Now, in order to calculate the final result for particular case of the Maxwell Boltzmann distribution (Eq. 6) we introduce the equivalent dimensionless expression to Eq. (11),

$$j(r_s) = (q_\alpha n_{\alpha o}) \pi c^4 \frac{1}{\pi^{3/2} c^3} \left[\int_0^{\hat{u}_s} \hat{u}^3 f_\alpha(\hat{u}) d\hat{u} + \left(\frac{r_p^2}{r_s^2} \right) \int_{\hat{u}_s}^\infty \hat{u}^3 f_\alpha(\hat{u}) \left(1 + \frac{|\hat{\phi}_p|}{\hat{u}^2} \right) d\hat{u} \right]$$

where $\hat{u}_s = v_s/c$. Then,

$$j(r_s) = (q_\alpha n_{\alpha o}) \frac{c}{\sqrt{\pi}} \left[\int_0^{\hat{u}_s} \hat{u}^3 e^{-\hat{u}^2} d\hat{u} + \left(\frac{r_p^2}{r_s^2} \right) \int_{\hat{u}_s}^\infty \hat{u}^3 e^{-\hat{u}^2} \left(1 + \frac{|\hat{\phi}_p|}{\hat{u}^2} \right) d\hat{u} \right]$$

and using the integrals,

$$\int_0^{\hat{u}_s} \hat{u}^3 e^{-\hat{u}^2} d\hat{u} = \frac{1}{2} \left[1 - e^{-\hat{u}_s^2} (1 + \hat{u}_s^2) \right]$$

$$\int_{\hat{u}_s}^\infty \hat{u}^3 e^{-\hat{u}^2} \left(1 + \frac{|\hat{\phi}_p|}{\hat{u}^2} \right) d\hat{u} = \frac{e^{-\hat{u}_s^2}}{2} \left[1 + \hat{u}_s^2 + |\hat{\phi}_p| \right]$$

this leads to,

$$j(r_s) = (q_\alpha n_{\alpha o}) \frac{c}{2\sqrt{\pi}} \left[1 + e^{-\hat{u}_s^2} \left(\left(\frac{r_p^2}{r_s^2} - 1 \right) + \hat{u}_s^2 \left(\frac{r_p^2}{r_s^2} - 1 \right) + \frac{r_p^2}{r_s^2} |\hat{\phi}_p| \right) \right]$$

The final expression is,

$$j(r_s) = (q_\alpha n_{\alpha o}) \frac{c}{2\sqrt{\pi}} \left[1 + \left(\frac{r_p^2}{r_s^2} - 1 \right) e^{-\hat{u}_s^2} \right] \quad (13)$$

and the collected current coincides with the Eq. (29) of Ref. [5],

$$I(r_p) = \frac{A_{sph}}{4} (q_\alpha n_{\alpha o}) V_{th} \frac{r_s^2}{r_p^2} \left[1 - \left(1 - \frac{r_p^2}{r_s^2} \right) \exp \left(-\frac{r_p^2}{r_s^2 - r_p^2} \frac{|q_\alpha \phi_p|}{K_B T_\alpha} \right) \right] \quad (14)$$

3.2 Cylindrical probe

The scheme with the motion of particles in the cylindrical geometry is represented in Fig. 12 where we assume the probe with a length $L \gg r_p$ much larger than its radius. As for the spherical probe, the velocity at r_p is \mathbf{v}' and \mathbf{v} at the radial distance $r > r_p$. The speed v_z along the Z axis is constant and the Fig. 10 also applies for the component $\mathbf{v}_\perp = \mathbf{v}_r + \mathbf{v}_\theta$ in the plane P perpendicular to the probe axis with $\mathbf{v}_\parallel \equiv \mathbf{v}$ (compare with Fig.12). Therefore,

$$\frac{m_\alpha}{2} (v_r^2 + v_\theta^2 + v_z^2) - q_\alpha \phi_p = \frac{m_\alpha}{2} (v_r'^2 + v_\theta'^2 + v_z^2)$$

The component L_z of the angular momentum is conserved,

$$\mathbf{L} = \mathbf{r} \wedge \mathbf{v}_\perp, \quad r v_\theta = r_p v'_\theta \quad \text{and} \quad v'_\theta = \frac{r}{r_p} v_\theta$$

and again we deduce a relation between the radial v_r and angular v_θ components in the plane P

$$\frac{v_r^2 - q_\alpha \phi_p / m_\alpha}{(r^2 / r_p^2 - 1)} \geq v_\theta^2$$

As for the spherical probe in Fig. 10 we have, $v_\theta = v_\perp \sin \varphi$ and $v_r = v_\perp \cos \varphi$,

$$\sin^2 \varphi_m \leq \frac{r_p^2}{r^2} \left(1 - \frac{2 q_\alpha \phi_p}{m_\alpha v_\perp^2} \right) \quad (15)$$

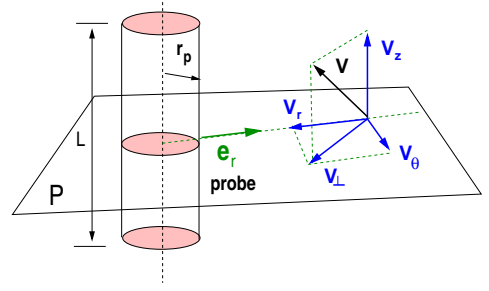


Figure 12: The geometry for the cylindrical probe.

This is the equivalent condition to Eq. (1) but only involves the component of the velocity v_\perp in the plane

P instead of $v = \sqrt{v_\perp^2 + v_z^2}$ as for the spherical probe. Again, two different situations arise for *attracted* and *repelled* particles.

3.2.1 Repelled particles

For repelled charges ($q_\alpha \phi_p > 0$) in Eq. (15) the particles require of a minimum speed $v_{\perp m} = \sqrt{2 q_\alpha \phi_p / m_\alpha}$ to reach the radial distance r_p . In addition, the maximum allowed value for φ is,

$$\sin \varphi_m = \pm \frac{r_p}{r} \sqrt{1 - \frac{2 q_\alpha \phi_p}{m_\alpha v_\perp^2}}$$

The current density over the surface element $d\mathbf{S}$ of Fig. 10 in the direction of the cylindrical probe is again,

$$dj(r) = q_\alpha v_r dn_\alpha = (q_\alpha n_{\alpha o}) (v_\perp \cos \varphi) f_\alpha(\mathbf{v}) d\mathbf{v}$$

with $d\mathbf{v} = dv_\perp dv_z$ therefore $d\mathbf{v} = v_\perp d\varphi dv_\perp dv_z$. Now, *assuming* again that the normalized energy distribution function is *isotropic* and that could be written as $f_\alpha(\mathbf{v}) = f_{\alpha\perp}(v_\perp) f_{\alpha z}(v_z)$ the current density becomes,

$$dj(r) = (q_\alpha n_{\alpha o}) \int_{v_\perp}^{\infty} v_\perp^2 f_{\alpha\perp}(v_\perp) dv_\perp \int_{-\varphi_m}^{+\varphi_m} \cos \varphi d\varphi \int_{-\infty}^{+\infty} f_{\alpha z}(v_z) dv_z$$

After the integration and using Eq. (15) we obtain,

$$j(r) = 2 (q_\alpha n_{\alpha o}) \frac{r_p}{r} \int_{v_{\perp m}}^{\infty} v_\perp^2 \sqrt{1 - \frac{2 q_\alpha \phi_p}{m_\alpha v_\perp^2}} f_{\alpha\perp}(v_\perp) dv_\perp \quad (16)$$

and the collected current is calculated as $I(r_p) = (2\pi r L) j(r)$.

$$I(r_p) = 2 A_{cyl} (q_\alpha n_{\alpha o}) \int_{v_{\perp m}}^{\infty} v_{\perp}^2 \sqrt{1 - \frac{2 q_\alpha \phi_p}{m_\alpha v_{\perp}^2}} f_{\perp \alpha}(v_{\perp}) dv_{\perp} \quad (17)$$

where $A_{cyl} = 2\pi r_p L$ is the surface of the probe.

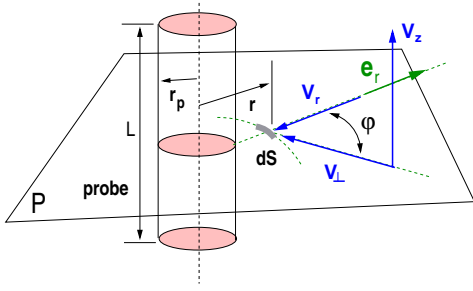


Figure 13: The velocity $\mathbf{v} = \mathbf{v}_{\perp} + \mathbf{v}_z$ of a charge over the surface element dS placed at the radial distance r .

For the particular case of the Maxwell Boltzmann distribution (Eq. 6) using the dimensionless velocity $\hat{u} = v_{\perp}/c$ as before,

$$j(r) = 2 (q_\alpha n_{\alpha o}) \frac{r_p}{r} \int_{\hat{u}_m}^{\infty} \hat{u}^2 e^{-\hat{u}^2} \sqrt{1 - \frac{\hat{\phi}_p}{\hat{u}^2}} d\hat{u}$$

and in this case,

$$\int_{\hat{u}_m}^{\infty} \hat{u}^2 e^{-\hat{u}^2} \sqrt{1 - \frac{\hat{\phi}_p}{\hat{u}^2}} d\hat{u} = \frac{\sqrt{\pi}}{4} e^{-\hat{u}_m^2}$$

The final values for the current density at the radial distance r is,

$$j(r) = \frac{r_p}{r} \frac{(q_\alpha n_{\alpha o}) V_{th}}{4} \exp\left(\hat{\phi}_p\right) = \frac{r_p}{r} \frac{(q_\alpha n_{\alpha o}) V_{th}}{4} \exp\left(\frac{q_\alpha \phi_p}{K_B T_\alpha}\right) \quad (18)$$

and the current collected by the probe is,

$$I(r_p) = \frac{(q_\alpha n_{\alpha o}) V_{th} A_{cyl}}{4} \exp\left(\frac{q_\alpha (V_p - V_{sp})}{K_B T_\alpha}\right) \quad (19)$$

Thus, for a Maxwellian plasma the current of repelled particle for spherical and cylindrical probes only differ by a geometrical factor, A_{sph} or A_{cyl} . Again, when the probe is biased to the plasma potential $\phi_p = 0$ and collects the thermal flow of particles,

$$I(V_p) = \frac{(q_\alpha n_{\alpha o}) A_{cyl}}{4} V_{th}$$

3.2.2 Attracted particles

For attracted charges $q_\alpha \phi_p < 0$ and the Eq. (15) becomes,

$$\sin^2 \varphi = \frac{r_p^2}{r^2} \left(1 + \frac{2 |q_\alpha \phi_p|}{m_\alpha v_{\perp}^2} \right) \quad (20)$$

which defines the radial distance $r_s > r_p$ and the critical speed $v_{\perp s}$. According to the velocity of the attracted charges, as for the spherical probe, the radial component of the current density at the distance r_s is the sum $dj(r_s) = dj_{sl}(r_s) + dj_{ol}(r_s)$ of the sheath limited and orbit limited parts. In this case using $v_r = v_{\perp} \cos \varphi$ and,

$$(dj)_r = dj(r_c) = q_\alpha v_r dn_\alpha = (q_\alpha n_{\alpha o}) (v_{\perp} \cos \varphi) f_\alpha(\mathbf{v}) d\mathbf{v}$$

Assuming an anisotropic velocity distribution function, with the details of the integration as indicated in Fig. 13,

$$j_{sl}(r_s) = (q_\alpha n_{\alpha o}) \int_0^{v_{\perp s}} v_{\perp}^2 f_{\alpha\perp}(v_{\perp}) dv_{\perp} \int_{-\pi}^{\pi} \cos \varphi d\varphi \int_{-\infty}^{+\infty} f_{\alpha z}(v_z) dv_z \quad (21)$$

and,

$$j_{ol}(r_s) = (q_\alpha n_{\alpha o}) \int_{v_{\perp s}}^{\infty} v_{\perp}^2 f_{\alpha\perp}(v_{\perp}) dv_{\perp} \int_{-\varphi_m}^{\varphi_m} \cos \varphi d\varphi \int_{-\infty}^{+\infty} f_{\alpha z}(v_z) dv_z$$

Using the Eq. (20) the integration leads to,

$$j(r_s) = 2(q_\alpha n_{\alpha o}) \int_0^{v_{\perp s}} v_{\perp}^2 f_{\alpha\perp}(v_{\perp}) dv_{\perp} + (q_\alpha n_{\alpha o}) \frac{r_p}{r_s} \int_{v_{\perp s}}^{\infty} v_{\perp}^2 \sqrt{1 + \frac{2|q_\alpha \hat{\phi}_p|}{m_\alpha v_{\perp}^2}} f_{\alpha\perp}(v_{\perp}) dv_{\perp} \quad (22)$$

The corresponding current is $I(r_p) = (2\pi r_s L) j(r_s)$. Because of the cylindrical symmetry, this last equation involves the *two dimensional velocity distribution function* $f_{\alpha\perp}(v_{\perp})$. The dimensionless Eq. (22) with $\hat{u} = v_{\perp}/c$ is,

$$j(r_s) = (q_\alpha n_{\alpha o}) \frac{2c}{\pi} \left[2 \int_0^{\hat{u}_s} \hat{u}^2 f_{\alpha\perp}(\hat{u}) d\hat{u} + \frac{r_p}{r_s} \int_{\hat{u}_s}^{\infty} \hat{u}^2 f_{\alpha\perp}(\hat{u}) \sqrt{1 + \frac{|\hat{\phi}_p|}{\hat{u}^2}} d\hat{u} \right]$$

and for the particular case of the two dimensional Maxwell Boltzmann distribution,

$$f_{2d}(\hat{u}) = \frac{2}{\pi c} e^{-\hat{u}^2}$$

we obtain,

$$j(r_s) = (q_\alpha n_{\alpha o}) \frac{2c}{\pi} \left[\int_0^{\hat{u}_s} \hat{u}^2 e^{-\hat{u}^2} d\hat{u} + \frac{r_p}{r_s} \int_{\hat{u}_s}^{\infty} \hat{u}^2 e^{-\hat{u}^2} \sqrt{1 + \frac{|\hat{\phi}_p|}{\hat{u}^2}} d\hat{u} \right]$$

The values of these integrals are,

$$\int_0^{\hat{u}_s} \hat{u}^2 e^{-\hat{u}^2} d\hat{u} = \frac{1}{4} \left[-2\hat{u}_s e^{-\hat{u}_s^2} + \sqrt{\pi} \text{Erf}(\hat{u}_s) \right]$$

$$\int_{\hat{u}_s}^{\infty} \hat{u}^2 e^{-\hat{u}^2} \sqrt{1 + \frac{|\hat{\phi}_p|}{\hat{u}^2}} d\hat{u} = \frac{e^{-\hat{u}_s^2}}{2} \sqrt{u_s^2 + |\hat{\phi}_p|} + \frac{\sqrt{\pi}}{4} e^{|\hat{\phi}_p|} \text{Erfc}(\sqrt{u_s^2 + |\hat{\phi}_p|})$$

where $\text{Erf}(x)$ and $\text{Erfc}(x)$ are the error and the complementary error functions. After some manipulations we obtain,

$$j(r_s) = \frac{1}{4} (q_\alpha n_{\alpha o}) V_{th} \left[\text{Erf}(\hat{u}_s) + \frac{r_p}{r} e^{|\hat{\phi}_p|} \text{Erfc}(\sqrt{\hat{u}_s^2 + |\hat{\phi}_p|}) \right] \quad (23)$$

and also for the current $I(r_p) = (2\phi r_s L) j(r_s)$,

$$I(r_p) = \frac{A_{cyl}}{4} (q_\alpha n_{\alpha o}) V_{th} \left[\frac{r_s}{r_p} \text{Erf}(\hat{u}_s) + e^{|\hat{\phi}_p|} \text{Erfc}(\sqrt{\hat{u}_s^2 + |\hat{\phi}_p|}) \right] \quad (24)$$

3.3 Approximations

For the particular case of the Maxwell Boltzmann velocity distribution the the results (Eqs. (7) and (18)) are equivalent and independent of the geometry of the probe for *repelled* particles. On the contrary, for *attracted* charges are different the Eqs. (13) for the spherical probe and Eqs.(23) for the cylindrical geometry ².

In addition, the above results for accelerating fields contains the radial distance r_s that could be identified with the *sheath edge*. This distance would mark the threshold between the bulk unperturbed plasma and the plasma sheath, as indicated in Figs. 5 and 6. In fact, such radius is undetermined as well as the plasma potential drop $\phi(r)$ around the probe. This calculation is complex and involves Poisson equation for the electric field around the probe, which is also influenced by the local spatial charge distribution in the sheath.

Therefore, some approximations are required to eliminate r_s from the above expressions for *attracted* particles. They compare the probe radius r_p with the radial distance r_s of the sheath limit. The *thin sheath* approximation corresponds to $r_s - r_p \gg r_p$ while in the *thick sheath limit* $r_s \gg r_p$.

3.3.1 The thin sheath limit

In this case the normalized speed,

$$\hat{u}_c^2 = |\hat{\phi}_p| \frac{r_p^2}{r_s^2 - r_p^2}$$

is large in the limit $r_s - r_p \gg r_p$. Thus, writing $I_{es} = A_{sph} (q_\alpha n_{\alpha o} V_{th})/4$ the Eq. 14 reads,

$$I(r_p) = I_{es} \frac{r_s^2}{r_p^2} \left[1 - \left(1 - \frac{r_p^2}{r_s^2}\right) e^{-\hat{u}_c^2} \right]$$

and using $\exp(-\hat{u}_c^2) \simeq 1$ we obtain,

$$I(r_p) \simeq I_{es} \frac{r_s^2}{r_p^2} \left(1 - 1 + \frac{r_p^2}{r_s^2} \right) = I_{es}$$

Therefore, the current of attracted particles for an spherical probe in the *thin sheath* limit is constant for bias voltages $V_p \gg V_{sp}$.

For the cylindrical probe, with $I_{es} = A_{cyl} (q_\alpha n_{\alpha o} V_{th})/4$ the Eq. 24 reads,

$$I(r_p) = I_{es} \left[\frac{r_s}{r_p} \text{Erf}(\hat{u}_c) + e^{|\hat{\phi}_p|} \text{Erfc}(\sqrt{\hat{u}_c^2 + |\hat{\phi}_p|}) \right] = I_{es} F(\hat{u}_c, |\hat{\phi}_p|)$$

and in the limit $r_s - r_p \gg r_p$ we may use of,

$$\text{Erfc}(x) = 1 - \text{Erf}(x) \simeq \frac{1}{\sqrt{\pi}} \frac{e^{-x^2}}{x}$$

²These expressions corresponds to Eqs. (29) and (30) in Ref. [5] and (43-49) in Ref. [7].

for large values of x . Thus, the function $F(\hat{u}_c, |\hat{\phi}_p|)$ can be approximated by,

$$F(\hat{u}_c, |\hat{\phi}_p|) \simeq \frac{r_s}{r_p} \left(1 - \frac{1}{\sqrt{\pi}} \frac{e^{-\hat{u}^2}}{\hat{u}} \right) + \frac{e^{|\hat{\phi}_p|} e^{-\hat{u}^2} e^{-|\hat{\phi}_p|}}{\sqrt{\pi} \sqrt{\hat{u}_c^2 + |\hat{\phi}_p|}}$$

And we have,

$$\hat{u}_c^2 + |\hat{\phi}_p| = |\hat{\phi}_p| \frac{r_p^2}{r_s^2 - r_p^2} + |\hat{\phi}_p| = \frac{r_s^2}{r_p^2} \hat{u}_c^2$$

After some simple manipulations we obtain,

$$F(\hat{u}_c, |\hat{\phi}_p|) \simeq \frac{r_s}{r_p} \left(1 - \frac{1}{\sqrt{\pi}} \frac{r_p^2}{r_s^2 - r_p^2} r_p^2 \frac{e^{-\hat{u}^2}}{\hat{u}} \right) \simeq \frac{r_s}{r_p} \sim 1$$

Therefore, in the *thin sheath limit* the current of attracted charges collected by both, the cylindrical and spherical probes $I = I_{es}$ is equal to the electron saturation current and independent of the probe bias for $V_p \gg V_{Sp}$.

3.3.2 The thick sheath limit

For the spherical probe when $r_s/r_p \gg 1$ we approximate,

$$\exp(-\hat{u}_c^2) = \exp \left[-|\hat{\phi}_p| \frac{1}{r_s^2/r_p^2 - 1} \right] \simeq \exp \left(-|\hat{\phi}_p| \frac{r_p^2}{r_s^2} \right) \sim 1 - |\hat{\phi}_p| \frac{r_p^2}{r_s^2}$$

and in Eq. (14) we have,

$$I(r_p) \simeq \frac{A_{sph}}{4} (q_\alpha n_{\alpha o}) V_{th} \left[\frac{r_s^2}{r_p^2} - \frac{r_s^2}{r_p^2} \left(1 - \frac{r_p^2}{r_s^2} \right) \left(1 - \frac{r_p^2}{r_s^2} |\hat{\phi}_p| \right) \right]$$

Writing $I_{es} = (A_{sph} q_\alpha n_{\alpha o} V_{th})/4$ we obtain,

$$I(r_p) \simeq I_{es} \left(1 + |\hat{\phi}_p| - \frac{r_p^2}{r_s^2} |\hat{\phi}_p| \right)$$

Finally, neglecting the small term,

$$I(r_p) \simeq I_{es} \left(1 + \frac{|q_\alpha \phi_p|}{K_B T_\alpha} \right) \quad (25)$$

In the *thick sheath limit* the collected current of attracted particles for the spherical probe grows linearly with the bias potential $V_p \gg V_{sp}$.

In the case of the cylindrical geometry,

$$F(\hat{u}_c, |\hat{\phi}_p|) = \frac{r_s}{r_p} \text{Erf}(\hat{u}_c) + e^{|\hat{\phi}_p|} \text{Erfc} \left(\frac{r_s}{r_p} \hat{u}_c \right)$$

and because $r_s \gg r_p$ for low values of \hat{u}_c we make use of $\text{Erf}(x) \simeq (2x)/\sqrt{\pi}$,

$$F(\hat{u}_c, |\hat{\phi}_p|) \simeq \frac{r_s}{r_p} \frac{2}{\sqrt{\pi}} \hat{u}_c + e^{|\hat{\phi}_p|} \text{Erfc}\left(\frac{r_s}{r_p} \hat{u}_c\right)$$

After some simple manipulations we obtain,

$$F(\hat{u}_c, |\hat{\phi}_p|) \simeq \frac{2}{\sqrt{\pi}} \sqrt{\hat{\phi}_p} + e^{|\hat{\phi}_p|} \text{Erfc}(\sqrt{\hat{\phi}_p})$$

On the contrary, the argument of $\text{Erfc}(\sqrt{\hat{\phi}_p}) \simeq \text{Erfc}(r_s \hat{u}_c / r_p)$ is large and we could make use of the previous approximation. Then,

$$F(\hat{u}_c, |\hat{\phi}_p|) \simeq \frac{2}{\sqrt{\pi}} \left(\sqrt{\hat{\phi}_p} + \frac{1}{2} \frac{1}{\sqrt{\hat{\phi}_p}} \right) \sim \frac{2}{\sqrt{\pi}} (1 + |\hat{\phi}_p|)^{1/2}$$

The final expression for the cylindrical probe is,

$$I(r_p) = I_{es} \frac{2}{\sqrt{\pi}} \left(1 + \frac{|q_\alpha \phi_p|}{K_B T_\alpha} \right)^{1/2} \quad (26)$$

For Maxwellian plasmas where the *thick sheath* approximation is valid, the Eqs. (25) and (26) suggest that $K_B T_\alpha$ could be determined by plotting I_p (or I_p^2) against $\phi_p = V_p - V_{sp}$. The density unperturbed density $n_{\alpha 0}$ also may be determined from the value of I_{se} .

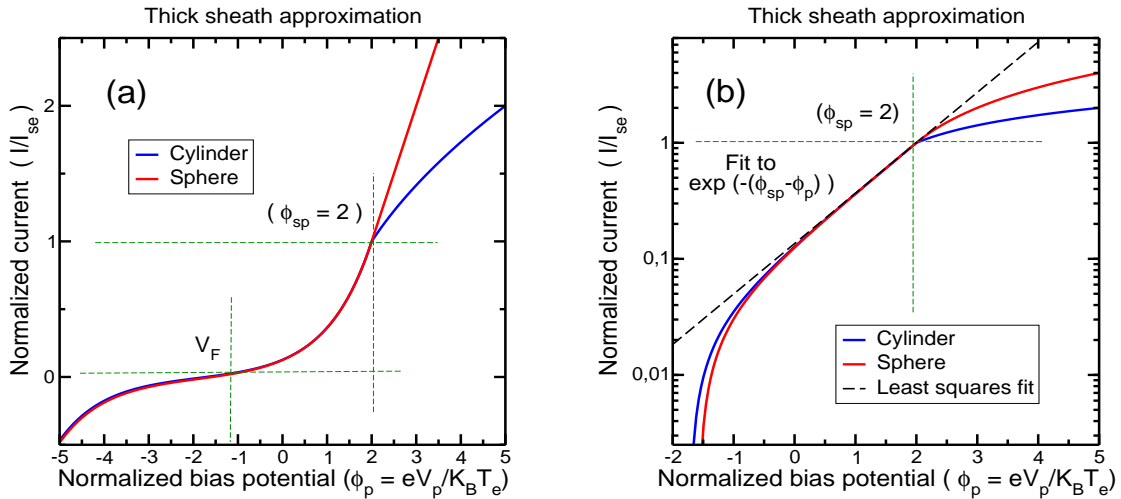


Figure 14: Comparison of the thick sheath approximation for spherical and cylindrical probes in (a) linear and in (b) logarithmic axis for an Argon plasma. The electron temperature is $K_B T_e = 3$ eV and the ion temperature $K_B T_i = 0.013$ eV (equivalent to the room temperature of 300 K). The plasma potential is $V_{sp} = 6$ V, ($\phi_{sp} = 2$ V with $\phi_{sp} = eV_{sp}/K_B T_e$).

The results of the *thick sheath* approximation for a typical plasma are represented in Fig. 14 and have a similar look to the idealized current voltage curve of Fig. 4. The curves also compare the Eq. (25) for spherical and Eq. (26) for cylindrical geometries. In the electron saturation region (*CD* in Fig. 4 where $V_p > V_{sp}$) the current is geometry dependent while this is not the case for repelled electrons (*AC* in Fig. 4 where $V < V_{sp}$). This fact is caused by the low temperatures and large mass of ions that increase for $V_p < V_{sp}$ the ion saturation current less than I_{se} for $V > V_{sp}$.

We conclude that the equations (25) and (26) lead to an important result. When the *thick sheath* approximation is valid in Maxwellian plasmas, the repelled particle temperature $K_B T_\alpha$ could be determined by plotting I_p (or I_p^2) against $\phi_p = V_p - V_{sp}$. Once $K_B T_\alpha$ is obtained, the plasma density $n_{\alpha 0}$ may be determined from the value of $I_{es} = A(q_\alpha n_\alpha) V_{Th}/4$.

However, as we shall see the validity of this approximation is limited when compared with actual experimental data (see Fig. 16 and the discussion in Sec. 4.1). In this *thick sheath* approximation the electric field around the probe remains undetermined because the Poisson equation has been ignored. Thus, more involved models are required to account for the orbital motion of attracted charges.

3.4 The energy distribution function of repelled particles

Finally, without making assumptions regarding the energy distribution function $g(E)$ and important result is deduced from Eqs. (4) and (17) for both geometries. [2, 9]. Deriving with respect of the lower limit of the integrals,

$$I(\alpha) = \int_a^b f(x, \alpha) dx$$

we have,

$$\frac{dI}{d\alpha} = f(b, \alpha) \frac{db}{d\alpha} - f(a, \alpha) \frac{da}{d\alpha} + \int_a^b \frac{\partial f(x, \alpha)}{\partial \alpha} dx$$

From Eq. (4) for the spherical probe we obtain,

$$I(r_p) = \frac{A_{sph} q_\alpha}{4} \int_{q_\alpha \phi_p}^{\infty} \left(1 + \frac{q_\alpha \phi_p}{E}\right) g(E) \sqrt{\frac{2E}{m_\alpha}} dE$$

Therefore,

$$\frac{d^2 I}{d\phi_p^2} = 0 - 0 + \int_{q_\alpha \phi_p}^{\infty} \frac{q_\alpha^2 \pi r_p^2}{E} \left(1 + \frac{q_\alpha \phi_p}{E}\right) g(E) \sqrt{\frac{2E}{m_\alpha}} dE$$

and,

$$\frac{d^2 I}{d\phi_p^2} = -(q_\alpha^2 \pi r_p^2) g(E) \sqrt{\frac{2q_\alpha}{m_\alpha \phi_p}}$$

We conclude distribution energy for *repelled* particles can be calculated from the second differential of the current with respect to the bias voltage,

$$g(E) = -\frac{1}{(q_\alpha^2 \pi r_p^2)} \sqrt{\frac{m_\alpha \phi_p}{2q_\alpha}} \left(\frac{d^2 I}{d\phi_p^2} \right)$$

This result is valid for *any geometry* as far as the velocity distribution is *isotropic*. Then, even for non Maxwellian plasmas, the distribution function of repelled particles $g(E)$ can be obtained from the experimental data. While this result is valid for any kind of repelled charge, in of particular interest for the electrons.

However High noise of the initial curve makes it very difficult to obtain the second differential of the current with respect to the bias voltage.

4 Interpretation of Langmuir probe data for repelling electrons

The above simplified theory considers an *isotropic equilibrium plasma* where none privileged direction for the particle speed exists. This is not the case for a large number of situations of physical interest where the probe and/or the plasma are in relative motion. However, the above theory only applies as far as the drift velocity of the plasma is low compared with the thermal speed of charges. This is also a common situations in low pressure discharge plasmas.

However, even when the energy distribution function is non Maxwellian, some important information could be obtained using collecting Langmuir probes. As we have seen, the repelled charges are collected over the surface S of the probe and Eq. (5) for the spherical and Eq. (16) for cylindrical geometry *are valid for any isotropic* velocity distribution function $f_\alpha(\hat{u})$.

In general, the repelled charge current of the specie α may be directly connected with $f_\alpha(\hat{u})$, this is of relevance for the *repelled electrons*. The electrons are mainly concerned because of the lower ion temperature, that leads the repelled ion currents to be one or two orders of magnitude much smaller than the electron currents in most experiments [2].

4.1 The analysis of experimental results

The classical analysis of the IV curves of collecting Langmuir curves is simple and based in the fact that Eqs. (8) and (19) are geometry independent. This calculation has been subject of a large number of refinements but its basic scheme has not been changed since the early work of Irvin Langmuir.

The first step is to subtract to all experimental data the value of the ion saturation current. This moves upwards the curve leading all currents positive. However, this value is frequently so small that this correction becomes negligible as for the experimental data shown in Fig. [15]. For low temperature plasmas where $T_i \ll T_e$ the ion saturation current is approximated close to the floating potential by the Bohm relation [4],

$$I_{is} = I_{Bohm} = 0.6 n_i e S \sqrt{\frac{K_B T_e}{m_i}}$$

The factor $0.6 = e^{-1/2}$ comes from the approximation of the plasma potential $V_{sp} \simeq K_B T_e / 2$ at the end of the presheath [4].

This expression comes from the fact that a positive space charge sheath can form only if the ion density is higher than the electron density at the sheath edge [4]. Furthermore, if the ion density shall decrease slower than the electron density the ions must approach the sheath with a speed exceeding the *Bohm velocity* [4],

$$v_B = \sqrt{\frac{K_B T_e}{m_i}}$$

To achieve this speed, an energy corresponding to a potential drop of $K_B T_e/2e$ before the plasma sheath is necessary. This accelerates the ions to speeds over the *ion sound speed* given by $c_{is} = \sqrt{K_B T_e/m_i}$.

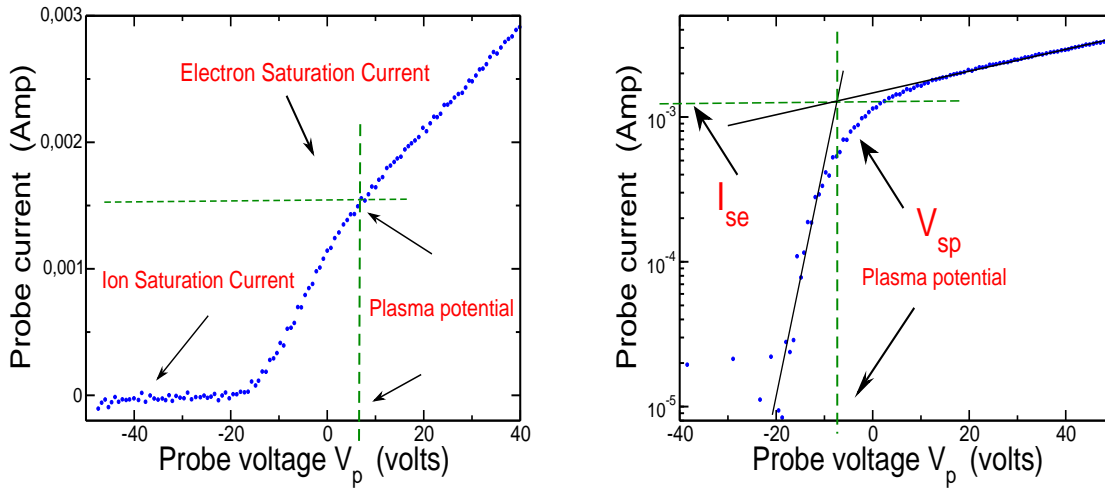


Figure 15: The graphical analysis of actual experimental current voltage curves of collecting Langmuir probes. These measurements could be compared with the theoretical predictions of Fig. [14].

Next, the electron temperature $K_B T_e$ is determined from the slope m of the exponential growth of the repelled electron current by least squares fitting of the experimental data as shown in Fig. [15].

The electron saturation current I_{se} is also estimated from the upper straight line corresponding to the fitting of the saturation current. The intersection of these two lines determines the plasma potential V_{sp} at the rounded knee of the curve. Finally, from Eqs. (9) and (19) the electron plasma density could be also calculated.

The sharp knee at the plasma potential and the flat ion and electron saturation curves in Fig. [4] are ideal probe features that are rarely seen in practice. The actual experimental data in Fig. [15] the real behavior with a rounded edge. In addition, with increasing bias voltage the ion and electron saturation curves also increments.

The rounded knee of Fig. [15] leads to imprecise determinations of the plasma parameters, in particular, the value of the plasma potential. This behavior is not theoretically predicted

in Fig. [14] for the *thick sheath* approximation where the effect of the local electric field is neglected. This suggests that the sheath formed around the probe would be responsible for this behavior.

Because of the electric imperfect probe shielding of electrons close to V_{sp} , the expansion of the plasma sheath is the more accepted explanation for this round off observed in Fig. 15 [1, 2].

However, this point is unclear, the plasma sheaths around the probe are small in weakly ionized plasmas with densities in the order of $\sim 10^8 \text{ cm}^{-3}$ and $T_e \approx 2 \text{ eV}$. The typical sheath thickness, in the order of the Debye length, are smaller than 0.1 mm [8], orders of magnitude below the typical size of the probe. Thus, the expansion of the sheath would produce a negligible increase in the collected current compared with those observed in the experiments.

On the contrary, for lower plasma densities and smaller probes the sheath expansion increases the collected current because the effective area for particles collection is the sheath and not the geometric probe area. Consequently, when the probe dimensions are comparable to the sheath thickness, the probe geometry has a larger influence on the IV characteristics.

This dependence of the current collected with the relative weight of each characteristic lengths (Debye length vs. probe size) and the actual extension of the perturbation introduced in the plasma (plasma sheath) remains as an open question.

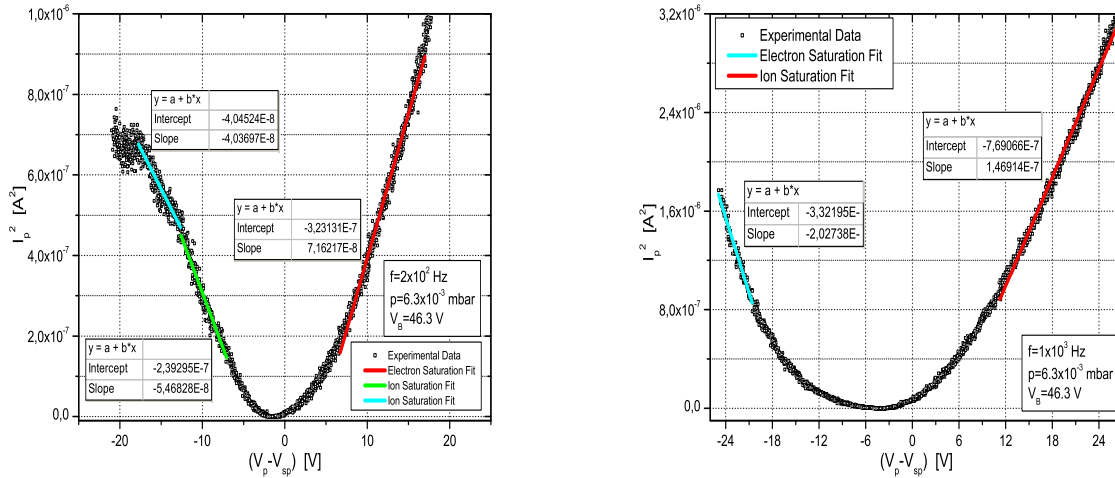


Figure 16: Comparison of the above graphical analysis with the thick sheath approximation for measurements using cylindrical probes.

Finally, the expressions obtained using the *thick sheath approximation* are compared in Fig. 16 with the values obtained from the graphical analysis of data in Fig. 15.

5 Emissive Langmuir probes

As discussed before, the plasma potential is determined from the IV curves of collecting

probes by the crossing point of two fitting lines. This method is prone to errors because of the round knee found in actual IV curves, as well as the noise observed for low values of the drained current in low density plasmas [3, 2]. The emissive probes are intended to provide reliable measurements of the plasma potential.

The emissive Langmuir probes are made of a thin wire immersed in the plasma and heated up by a DC or AC currents. This heated filament is biased as a collecting probe as shown in the scheme of Fig. 17.

The current I_h heats the wire up to red glow within temperature range of 1700-2000 K as in Fig. 18. This produces the thermal emission of an electron current given by the Schottky-Richardson formula [3, 2],

$$j_{e,Th} = C T_w^2 \exp\left(-\frac{e W_f}{K_B T_w}\right) \quad \text{and,} \quad I_{em} = S \times j_{e,Th} \quad (26)$$

where S is the surface of the wire, T_w is the filament temperature, W_f the work function of the metal and the constant $C = 6.02 \times 10^5 \text{ A/m}^2\text{K}^2$. This emitted electron current essentially depends on the temperature T_w of the filament.

Therefore, when the probe is biased more positive than the local plasma potential $V_p > V_{sp}$ the emitted electrons are reflected back to the probe. On the contrary, if the bias potential is negative with respect to the surroundings $V_p < V_{sp}$ the electrons can escape to the plasma and appear as an effective ion current. The interpretation of emissive probe data is based on the separation of the hot and cold IV traces that occurs near the plasma potential. This electron emission process is not sensitive to the plasma flow because only depends on the local plasma potential, rather than the electron kinetic energy. However, emissive probes do not provide useful data on plasma density and temperature as collecting probes.

Although emissive probes have been investigated for a long time there still remain many controversial issues regarding the emitted electron current and the space charge effects. In accordance to the magnitude of the current given by Eq. (5) the emissive probes operate in two different regimes. The *strong emission regime* ($I_{e,Th}/I_{es} > 1$) occurs when the thermal electron current is higher than the electron saturation current I_{es} collected by the cold probe. In this case charge space effects around the wire are important while could be neglected in the opposite *weakly emission limit* ($I_{e,Th}/I_{se} < 1$).

5.1 Floating emissive probe

For probes operating in the *low emission mode*, the current I_{hw} from a heated wire could be written as [2, 11],

$$I_{hw} = \begin{cases} -(I_{em} + I_{si}) & V_p \leq V_{sp} \\ -I_{em} G(V_p - V_{sp}) \exp\left[-\frac{e(V_p - V_{sp})}{K_B T_w}\right] & V_p > V_{sp} \end{cases}$$

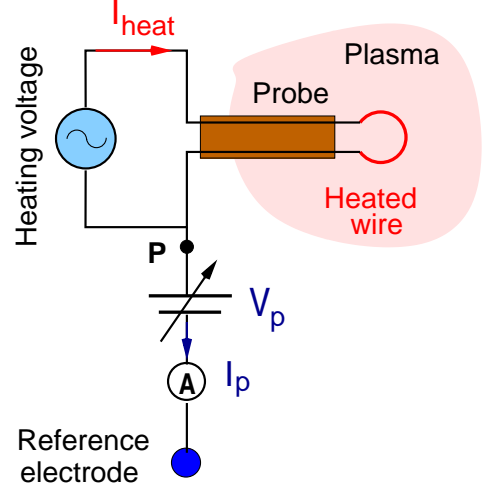


Figure 17: Scheme of the basic electrical connections of an emissive probe.

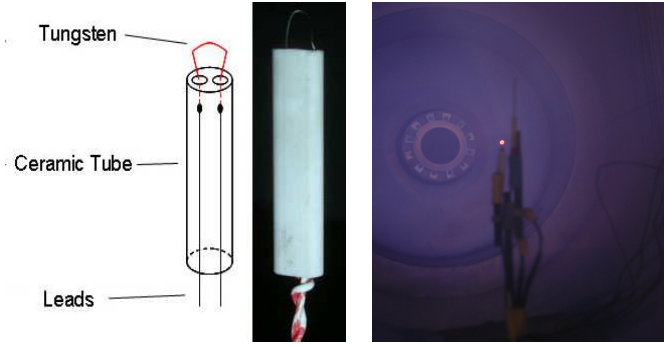


Figure 18: The picture and scheme of an emissive probe (left) and this probe operating in a glow discharge plasma (right).

Here, I_{em} is the electron thermal current of Eq. (5) and I_{is} the ion saturation current. The electron thermal emission depends on the temperature of the wire T_w and is considered as constant for $V_p \leq V_{sp}$ and decreasing for $V_p > V_{sp}$. The same filament for low T_w , acting as a cylindrical *cold probe* collects the current I_{cw} also approximated by,

$$I_{cw} = \begin{cases} I_{es} G'(V_p - V_{sp}) & V_p \geq V_{sp} \\ I_{se} \exp\left[\frac{e(V_p - V_{sp})}{K_B T_e}\right] & V_p < V_{sp} \end{cases}$$

where I_{se} is the electron saturation current. The factors $G'(V_p - V_{sp})$ and $G(V_p - V_{sp})$ account for the orbital motion of electrons and could be approximated [2] using the *thick sheath* model of Eq. (26).

The heated probe combines the emission and collection processes and the total collected current is $I(V_p) = I_{cw} + I_{hw}$, and writing $\phi_p = (V_p - V_{sp})$ for $\phi_p < 0$ we obtain,

$$I_p(\phi_p) = I_{se} e^{(e\phi_p/K_B T_e)} - (I_{em} + I_{si})$$

The first term is the exponential increase of the electron current when V_p approaches V_{sp} , which is reduced by a constant negative electron emission current. For the floating potential $I(V_F) = 0$ of the probe,

$$I_{se} e^{(e\phi_F/K_B T_e)} = I_{em} + I_{si}$$

taking the logarithm in both sides,

$$\ln\left(\frac{I_{em} + I_{si}}{I_{se}}\right) = \frac{e\phi_F}{K_B T_e}$$

Finally, we obtain,

$$V_{sp} = V_F - \frac{K_B T_e}{e} \ln \left(\frac{I_{em} + I_{si}}{I_{se}} \right)$$

In the *weak emission* regime $I_{em} + I_{si} < I_{se}$ and $\ln(I_{em} + I_{si}/I_{se}) < 1$ and finally,

$$V_{sp} = V_F + \frac{K_B T_e}{e} \ln \left(\frac{I_{se}}{I_{em} + I_{si}} \right) > V_F \quad (26)$$

This last equation permits to determine V_{sp} using the *floating potential* of the emissive probe. The emission current I_{em} increases with the temperature of the wire (Eq. (5)) when $I_{em} \simeq I_{se}$ the logarithm in Eq. (5.1) is very small and $V_{sp} \simeq V_F$. Therefore the potential of a *floating emissive probe* is very close to the value of the plasma potential.

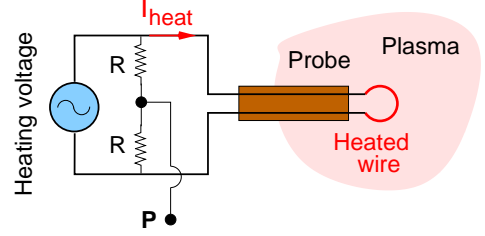


Figure 19: Symmetric emissive probe circuit.

There is an inevitable voltage drop ΔV along the hot wire which limits the accuracy of the measurements of V_{sp} . The circuit of Fig. 19 is employed to improve the readings biasing the point P . The signal from the probe is connected to the same point in the scheme of Fig. 17.

5.2 The inflection point method

Procedures which involve significant electron emission, such as the floating potential method, perturbs the local surrounding of the probe. This is of particular concern in low density plasmas where the emitted electron current may perturb the local electron density.

Ref. [11] introduces the *inflection point method* to determine the plasma potential more accurately. Because this is a quite sophisticated technique, which involves the numerical differentiation of the experimental data it will not be considered in this work.

The principal idea of the inflection point technique is to follow the inflection point of the IV characteristics as the emission is decreased down to the point of zero emission. When space charge effects can be neglected, the inflection point corresponds to the plasma potential. Therefore, the inflection point is determined by the derivative dI/dV_b . There, where the slope of the curve changes the inflection point can be found.

The total probe current I_p for $V_p \leq V_{sp}$ is,

$$I_p = I_{se} \exp \left[\frac{e(V_p - V_{sp})}{K_B T_e} \right] - (I_{em} + I_{is})$$

and for $V_p > V_{sp}$,

$$I_p = I_{se} \left[1 + \frac{e(V_p - V_{sp})}{K_B T_e} \right]^{1/2} - I_{em} \exp \left[\frac{-e(V_p - V_{sp})}{K_B T_w} \right] \left[1 + \frac{e(V_p - V_{sp})}{K_B T_w} \right]^{1/2}$$

Differentiating both equations for I_p with respect to V_p gives,

$$\frac{dI_p}{dV_p} = \frac{e I_{se}}{K_B T_e} \exp \left[\frac{e(V_p - V_{sp})}{K_B T_e} \right]$$

and

$$\begin{aligned} \frac{dI_p}{dV_p} = & \frac{e I_{se}}{K_B T_e} \frac{1}{2} \left[1 + \frac{e V_p}{K_B T_e} \right]^{-1/2} - \frac{e I_{em}}{K_B T_w} \exp \left[\frac{-e(V_p - V_{sp})}{K_B T_w} \right] \times \\ & \times \left[\left(\frac{1}{2} + \frac{e V_p}{K_B T_w} \right)^{-1/2} - \left(1 + \frac{e V_p}{K_B T_w} \right)^{-1/2} \right] \end{aligned}$$

When these equations are plotted for an ideal cylindrical probe, the plasma potential can be determined by the sharp peak for $V_b \sim V_{sp}$.

It is difficult to determine the small peak of the slope in the derivation because of the noise. It is determined by observing the moving peak by varying the emission. Ref. [2] found that space charge effects can be reduced by decreasing probe radius. With increasing radius the radial electrical field decreases and the shift becomes greater

References

- [1] I.M. Hutchinson. Principles of plasma diagnostics. (Cambridge University Press, Cambridge, 1987) Chap. 3.
- [2] N. Hershkowitz. How Langmuir probes work. in *Plasma Diagnostics. Discharge parameters and chemistry*, Vol. 1 ed. by O. Auciello and D.L. Flamm (Academic Press, Boston, 1989), Chap. 3.
- [3] Y.P. Raizer, *Gas Discharge Physics*. (Springer Verlag, Berlin, 1991). Chaps. 6 and 8.
- [4] F.F. Chen. Introduction to plasma physics and controlled fusion. Vol. 1: *Plasma physics*. 2nd edition (Plenum Press, New York, 1984).
- [5] L. Schott. Electric probes in *Plasma Diagnostics*, ed. by W. Lochte-Holtgreven (Elsevier, New York, 1968), Chap. 11.
- [6] F.F. Chen. Lecture notes on Langmuir probe diagnostics. Mini course on plasma diagnostics, IEEE-ICOPS meeting. Jeju, Korea (2003). Available from the web page of the author: <http://www.ee.ucla.edu/~ffchen/Publs/Chen210R.pdf>.
- [7] F.F. Chen. Electric Probes. in *Plasma Diagnostic Techniques*. R.H. Huddlestone and S.L. Leonard, Editors. (Academic Press, New York), Chapter 4, pp. 113-200 (1965). Available from the web page of the author: <http://www.ee.ucla.edu/~ffchen/Publs/Chen210R.pdf>.
- [8] R.L. Merlino. Understanding Langmuir probe current-voltage characteristics. *Amer. J. Phys.* **75**, (12), pp. 1078-1085 (2007).

- [9] J.E. Allen. Probe Theory - The orbital motion approach. *Physica Scripta*. **45**, pp. 497-503 (1992).
- [10] R.F. Kemp and J.M. Sellen. Plasma potential measurements by electron emitting emissive probes. *Rev. Sci. Instrum.* **35**, (4), pp. 455-461 (1966).
- [11] J.R. Smith, N. Hershkowitz and P. Coakley, Inflection point method of interpreting emissive probe characteristics. *Rev. Sci. Instrum.* **50**, (2), pp. 210-218 (1979).